Appl. Phys. B 85, 375–382 (2006)
DOI: 10.1007/s00340-006-2411-y

Applied Physics B
Lasers and Optics

J.T. HODGES[1,✉]
D. LISAK[1,2]

Frequency-stabilized cavity ring-down spectrometer for high-sensitivity measurements of water vapor concentration

[1] Chemical Science and Technology Laboratory, National Institute of Standards and Technology, 100 Bureau Drive, Gaithersburg, Maryland, MD 20899, USA
[2] Instytut Fizyki, Uniwersytet Mikołaja Kopernika, ul. Grudziadzka 5/7, 87-100 Toruń, Poland

Received: 19 June 2006/Revised version: 18 July 2006
Published online: 12 August 2006 • **© Springer-Verlag 2006**

ABSTRACT We present a portable spectrometer that uses the frequency-stabilized cavity ring-down spectroscopy technique capable of high-precision measurements of trace water vapor concentration. Measuring one of the strongest rovibrational transitions in the $\nu_1 + \nu_3$ water vapor combination band near $\tilde{\nu} = 7181.156\,\mathrm{cm}^{-1}$, we compare spectroscopic and thermodynamic determinations of trace water vapor in N_2, and find systematic differences attributable to water vapor background effects and/or uncertainties in line intensities. We also compare the frequency-stabilized ring-down method with other cavity ring-down approaches that are based on unstabilized probe lasers and unstabilized ring-down cavities. We show that for the determination of water vapor concentration, the frequency-stabilized cavity ring-down method has the minimum measurement uncertainty of these techniques. The minimum noise-equivalent absorption coefficient of the spectrometer was $1.2 \times 10^{-10}\,\mathrm{cm}^{-1}\,\mathrm{Hz}^{-1/2}$, which further corresponds to a minimum detectable water vapor mole fraction equal to 0.7×10^{-9} for an absorption spectrum of 10 minutes duration.

PACS 33.20.-t; 33.70.Jg; 33.70.Fd; 42.62.Fi

1 Introduction

New gas standards that are based upon quantitative laser absorption spectroscopy and exploit recent advances in measurement techniques and laser technology are being developed for a number of low-molecular weight species, including water vapor. There are numerous scientific and industrial applications that demand low-uncertainty and high-sensitivity humidity measurements. Examples include water vapor concentration measurements in the atmosphere [1], in products of combustion [2, 3], and in high-purity specialty process gases [4] used for the fabrication of semiconductor and photonics devices. To address these and other measurement needs, the National Institute of Standards and Technology (NIST) maintains primary methods of water vapor generation and measurement [5] and disseminates these standards through reference data and calibrations of related transfer standards.

Unlike the situation for many other stable species, low-range water vapor concentration standards are not provided as gravimetrically prepared, value-assigned mixtures in closed containers. This is because water adsorbs readily to the walls of most vessel materials, an effect so important that the water vapor concentration in a static charge cannot be known with confidence based on gravimetric methods alone. Thus, flowing gas streams, which help mitigate undesired wall effects, are required to achieve low concentrations of water vapor in process gases. For standards of trace water vapor generation, samples are prepared using thermodynamic-based humidity generators or with calibrated permeation tube/flow dilution systems [5]. These methods can be used to deliver known quantities of water vapor and to calibrate continuous sampling hygrometers, such as quartz-crystal microbalances, electrolytic- and capacitive-based sensors and chilled-mirror hygrometer (CMH) instruments [4]. Of these hygrometers, CMHs, which measure water vapor content in terms of the water vapor condensation temperature of the sample gas stream, provide the most fundamental and accurate measure of water vapor concentration. Although highly reliable and precise, these devices cannot be used with reactive or corrosive gases, are relatively slow and must work at or near atmospheric pressure with detection limits of water vapor mole fraction at the 10^{-8} level. In contrast, techniques based on quantitative absorption spectroscopy can directly measure water vapor concentration in a static charge or steady flow configuration, and therefore overcome ambiguities associated with changing gas mixture composition. Spectroscopic methods are also applicable to a wide variety of mixtures, are species selective, and potentially rapid.

In this article we describe a portable spectrometer based upon the frequency-stabilized cavity ring-down spectroscopy (FS-CRDS) technique, and we compare the accuracy of this to two other commonly used CRDS methods. We also compare FS-CRDS and CMH measurements of water vapor concentration, the latter being directly linked to NIST primary humidity standards. Finally we discuss the emerging role of FS-CRDS

✉ Fax: +1 301 869-5924, E-mail: joseph.hodges@nist.gov

as a primary method for measuring the absolute concentration of water vapor and other gases.

2 Measurement technique

2.1 *Sample absorption spectrum*

We consider a dilute mixture of water vapor in a carrier gas, where the absorption coefficient is given by $\alpha(\nu) = n \sum \sigma_i(\nu)$ and where n is the water vapor concentration, ν is the radiation frequency of the probe laser, σ_i is the absorption cross section associated with transition i, and the summation is over all relevant absorption transitions. Furthermore, σ_i can be expressed as $\sigma_i(\nu) = g_i(\nu - \nu_i) S_i c$ where ν_i is the frequency of transition i, $g_i(\nu - \nu_i)$ is the line shape function associated with the mixture of water vapor and carrier gas, S_i is the corresponding line intensity and c is the speed of light. For the low-pressure, near-infrared rovibrational water vapor spectra reported here, $\alpha(\nu)$ can usually be modeled as the sum over a small number of absorption transitions, with more distant transitions only contributing a slightly sloped pedestal to the spectrum. In the absence of line mixing effects, $\int \mathrm{d}\nu g_i(\nu) = 1$, so that integration of the cross-section over frequency yields the line intensity. It follows that the line area can be defined as the integral $\mathcal{A}_i = \int \mathrm{d}\nu \alpha_i(\nu) = n S_i c$, thus providing a simple relationship between the observed spectrum and water vapor concentration and line intensity. As shown below, the quantities $\mathcal{A}_i$ are determined by fitting physically appropriate line shapes to the measured absorption spectrum to yield the measured values for nS_i. For known S_i and measured $\mathcal{A}_i$ the CRDS-measured water vapor mole fraction is given by $x_{\mathrm{CRDS}} = (\mathcal{A}_i S_i^{-1} c^{-1})(k_\mathrm{b} T p^{-1})$, where the gas mixture is assumed to be ideal and in which k_b, T and p represent the Boltzmann constant, and gas temperature and pressure, respectively.

2.2 *Cavity ring-down spectroscopy*

Cavity ring-down spectroscopy (CRDS) was introduced nearly twenty years ago [6], and in the past decade has emerged as a powerful technique that has enabled absorption spectroscopy of many species, including weakly absorbing gases [7, 8], liquids [9], and aerosols [10, 11]. CRDS has several attributes which make it attractive for hygrometry, including low detection limits, compact sample volumes, and insensitivity to fluctuations in laser power and absorption of the source laser beam by ambient water vapor. The visible and near-infrared absorption spectrum of H_2O comprises thousands of discrete rovibrational transitions spanning several decades in intensity, thus giving a wide dynamic range and selectivity.

In CRDS one measures the decay time of recirculating light intensity within a resonant optical cavity, known as a ring-down cell. This resonator is typically a Fabry–Pérot interferometer formed by a pair of highly reflecting and partially transmitting dielectric mirrors. Assuming excitation of a single-cavity mode, the time dependence of light intensity leaking out of the cavity is an exponential decay, and can be characterized by its decay rate given by $\tau^{-1} = c[T_\mathrm{m}\ell^{-1} + \alpha(\nu)]$. Here τ is the ring-down cavity time constant, T_m is the effective transmission of the mirrors, ℓ is the cavity length, and $\alpha(\nu)$ corresponds to the absorption coefficient of the sample between the cavity mirrors. From this simple relation and by treating the quantity $cT_\mathrm{m}\ell^{-1}$ as a well-behaved baseline term in the spectrum $\tau^{-1}(\nu)$, $\alpha(\nu)$ can be determined by measuring the change above the baseline in the cavity decay rate. To quantify the sensitivity of CRDS, we define the noise-equivalent absorption coefficient to be $\sqrt{2/f_\mathrm{a}}\ \sigma_\tau/(c\langle\tau\rangle^2)$, where σ_τ is the standard deviation of the cavity time constant, $\langle\tau\rangle$ is the ensemble mean time constant and f_a is the ring-down signal acquisition rate.

The term CRDS refers to a wide variety of sensitive absorption techniques, and consequently any discussion regarding the performance of CRDS needs to acknowledge its different implementations. With regard to measurement accuracy, there are important differences between specific CRDS techniques. The earliest implementations of CRDS used pulsed probe lasers with bandwidths which were usually much greater than the cavity mode spacing and which were significant compared to transition line widths [6, 12, 13]. Complications arising from multi-mode excitation and bandwidth effects were investigated and limitations of this relatively broadband approach precluded low uncertainty measurements of line shapes and line intensities [14–16]. Subsequently single-mode pulsed CRDS experiments with frequency-stabilization which mitigated multi-mode complications were developed to yield low-uncertainty line intensities for O_2 [17, 18]. CRDS is now typically implemented with relatively narrow bandwidth single-mode continuous-wave (cw) lasers [19–22]. However, in cw-CRDS, the excitation of spectrally narrow ring-down cavity resonances by a narrow bandwidth source laser requires strategies for controlled cavity excitation. Also, cw-CRDS measurements of near-infrared water vapor spectra have been reported [23, 24], and a cw-CRDS instrument for trace water vapor measurement is now commercially available [25].

Frequency-stabilized cavity ring-down spectroscopy (FS-CRDS) uses the comb of resonant frequencies associated with a ring-down cavity to provide a well-defined frequency detuning axis for cavity ring-down absorption spectra, and this comb is actively stabilized using a frequency-stabilized reference laser. Sample absorption is measured using a cw probe laser with a bandwidth substantially smaller than the free-spectral-range (FSR) of the ring-down cavity. This narrow bandwidth excitation of the ring-down cavity enables one to readily select the fundamental transverse mode of the ring-down cavity (TEM_{00}) without having to achieve near-perfect mode matching. In practice the TEM_{00} is excited at each frequency step, the probe laser is actively frequency locked to this resonance and finally by rapidly switching off the intensity of the cw probe laser the passive exponential decay of light intensity emitted by a single mode of the ring-down cavity is observed. As recently demonstrated [26], the FS-CRDS method provides a frequency resolution approaching the ring-down cavity line width ($\simeq 50$ kHz) and excellent linearity in the frequency axis; attributes making this method suitable for high-precision measurements of line shape and line shifting effects as well as non-linear saturation effects. More detailed descriptions of the FS-CRDS method can be found in [26–28].

3 Experimental apparatus

The FS-CRDS measurements presented here were made with a setup which is nearly identical to that described in [27, 28], with the primary exception being a new probe laser consisting of a single-mode fiber-pigtailed distributed-feedback diode laser (DFB) emitting approximately 20 mW of power in the wavelength range $\lambda = \tilde{\nu}^{-1} = 1.392\,\mu\text{m}$ with a line width approaching 1 MHz. Lasers of this type were developed for gas sensing applications and are now commercially available for probing water vapor and other gases in the near-infrared region. Also, unlike the previously described FS-CRDS system, the apparatus was mounted upon a cart with a $0.9\,\text{m} \times 1.2\,\text{m}$ optical breadboard to enable portability of the spectrometer. See Fig. 1. As in [26–28] we stabilized the ring-down cavity length ($\ell \simeq 74$ cm) using a 633 nm frequency-stabilized HeNe reference laser (absolute frequency stability of 1 MHz) and a transmission lock. We measured a FSR of 202.8(1) MHz, giving a standard relative uncertainty in the frequency detuning axis less than 0.05%. Ring-down cavity mirrors with $T_\text{m} \simeq 2.5 \times 10^{-4}$ at the probe wavelength were used. To generate absorption spectra, the probe laser was frequency locked to the TEM_{00} transverse mode of the frequency-stabilized ring-down cavity at each frequency step in the absorption spectrum, and a set (typically 100) of ring-down signals was acquired and digitized with a 12 bit A/D board at 25 Msamples s^{-1} and fit in real-time using a fast least-squares algorithm [29]. The spectral acquisition proceeded by temperature tuning the probe laser to successive longitudinal cavity modes, followed by relocking of the laser to the cavity and ring-down signal acquisition. All measurements were made at room temperature. The cell temperature was continuously measured and changes of cell temperature were typically less than $0.1\,\text{K}\,\text{h}^{-1}$.

The water vapor sample in N_2 carrier gas was generated using a permeation tube moisture generation (PTMG) apparatus to provide sample gas to the FS-CRDS spectrometer and to a high-precision CMH. These two water vapor measurement systems were located in parallel downstream of the PTMG. Volumetric flow rates ranging from 0.5 std. L min^{-1} to 1.8 std. L min^{-1} and 0.25 std. L min^{-1} to 0.5 std. L min^{-1} were maintained through the ring-down cell and CMH, respectively. The ring-down cell pressure was actively regulated to within 0.1% and the CMH sample gas pressure was nominally atmospheric. All measurements were taken on gas samples containing nominal mole fractions of water vapor in N_2 in the range 2×10^{-6} to 4.5×10^{-6}. The CMH (frost-point $u(T_\text{f}) < 50$ mK) was calibrated directly against a primary thermodynamic humidity generator maintained at NIST [5] to measure the mole fraction, x of water vapor in N_2 produced by the PTMG. Ancillary data acquired at each step included T and p measured at the ring-down cavity, and the frost-point temperature T_f and pressure p_f of the sample gas in the CMH. The CMH-measured water vapor mole fraction was given by $x_\text{CMH} = f(T_\text{f}, p_\text{f}) e_\text{w}(T_\text{f})/p_\text{f}$ where f is the enhancement factor for mixtures of water vapor and N_2 [30] and e_w is the saturation vapor pressure of ice [31]. The standard relative uncertainty in x_CMH was estimated to be 0.7%.

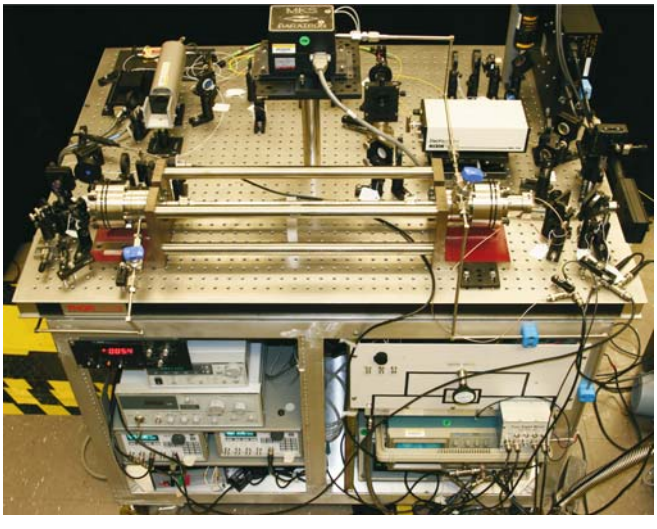

FIGURE 1 Photograph of portable frequency-stabilized ring-down apparatus. Data acquisition system not shown

4 Results

4.1 *Comparison of* cw *cavity ring-down techniques*

Here we consider two other approaches to cw-CRDS and compare them to FS-CRDS. The first approach, which we call multi-mode CRDS (MM-CRDS), is applied in the widely used commercial CRDS system [25] and uses an unstabilized ring-down cavity with no frequency lock between the cavity and probe laser. This method relies on the modulation of the probe laser frequency by an amount exceeding the cavity FSR. This is done to force the laser and cavity frequencies to periodically overlap and force the pumping of the ring-down cavity, thus enabling continuous data acquisition at any relative detuning of the laser and cavity modes. Spectra are acquired by slowly ramping or step-scanning the laser frequency along with a superimposed modulation. In MM-CRDS although one cavity mode at a time is excited, within the ensemble of ring-down signals acquired at each value of the probe-laser frequency ramp there are shot-to-shot variations in ring-down decay signals arising from the fact that different longitudinal cavity modes (and possibly different transverse modes) can be excited. As shown below, this causes compromised measurement statistics, line shape distortion and a spectral resolution limited by the cavity FSR. The second approach, which we call single-mode CRDS (SM-CRDS) lacks an absolute frequency reference as in FS-CRDS [32–34] but typically incorporates frequency locking of the cavity to the probe laser or vice versa. In SM-CRDS the frequency detuning of the probe laser is measured in terms of the calibrated frequency tuning of the laser, or by an external étalon, a wavemeter or by measuring the transition frequencies of known spectra and using these features for interpolation of the frequency axis [22]. The SM-CRDS can be also realized without any locking scheme by modulation of the ring-down cavity resonance frequency over a range exceeding the cavity FSR while keeping the laser at constant frequency [21, 23]. However this unlocked scheme requires better modematching of the probe laser beam to a single transverse mode of the cavity than for the frequency-locked SM-CRDS case. This condition is required to avoid excitation of

more than one transverse mode while scanning the cavity. We note that ring-down signals of different transverse modes have different time constants. The acquisition rate for the unlocked SM-CRDS case is also lower than in the frequency-locked case SM-CRDS case. In general, the frequency-locked SM-CRDS approach yields an improved frequency axis over MM-CRDS and avoids the multi-mode excitation problem. However even in frequency-locked SM-CRDS effects such as laser frequency drift, nonlinearities in probe laser tuning and frequency drift in external étalons can contribute to slow variation and distortion of measured spectra.

To quantify differences between the MM-CRDS, SM-CRDS and FS-CRDS methods, we measured the $\tilde{\nu} = 7181.156\,\mathrm{cm}^{-1}$ water vapor transition at identical conditions. For the MM-CRDS spectra, we turned off the ring-down cavity frequency lock, and we modulated the DFB laser current with a 10 Hz triangle wave to produce a peak-to-peak laser frequency modulation equal to $1.25 \times \mathrm{FSR}$. The mean laser frequency was temperature tuned in steps of 1 FSR. For the frequency-locked SM-CRDS spectra, the ring-down cavity was unlocked with respect to the frequency-stabilized HeNe used for absolute stabilization of the ring-down cavity. However, we locked the DFB laser frequency to sequential longitudinal mode orders of the ring-down cavity TEM_{00} as in the FS-CRDS method. Acquisition times for individual scans were $\simeq 10$ min. Figure 2 summarizes results for the condition $p = 13.3$ kPa. This figure shows a set of three absorption spectra and Galatry [35] line shape fits for each case (top panel), and shows fit residuals (middle panel) and relative standard deviations (bottom panel) in τ for selected spectra. The MM-CRDS measurements exhibit the poorest repeatability and greatest distortion of line shape. The MM-CRDS fit residuals exhibit a complicated structure arising from the uncontrolled excitation of adjacent TEM_{00} mode orders as the probe laser is tuned over the absorption transition. This effect is also manifest in the bottom panel case. Here the relative standard deviation given by $\sigma_\tau/\langle\tau\rangle$ is strongly frequency dependent and approaches 10% near the region of maximum slope in the absorption line. In contrast $\sigma_\tau/\langle\tau\rangle$ values are nearly frequency-independent for the SM-CRDS and FS-CRDS spectra; a consequence of single-mode excitation of the ring-down cavity. Although the short-term statistics for the SM-CRDS and FS-CRDS are similarly given by $\sigma_\tau/\langle\tau\rangle \simeq 0.2\%$, inspection of the three SM-CRDS spectra reveals a drift in the cavity resonance frequencies arising from slow thermal expansion effects. This slow drift degrades the linearity of the SM-CRDS frequency axis and produces a small but measurable distortion of the observed line shape. Indeed, for the FS-CRDS spectra, the fit-residuals are within the noise level of the observations, and the mean-square residual δ^2 is $\simeq 3.5$ times lower than that of the SM-CRDS spectra.

A common strategy for monitoring gas concentration is to probe the peak of a pressure-broadened absorption transition since many applications require fast time response. In Fig. 3 we present the time response of the respective MM-CRDS, SM-CRDS and FS-CRDS signals at $p = 93.3$ kPa, each taken over the course of more than 1 h on identical samples. The MM-CRDS measurements exhibit short and long-term fluctuations arising from the motion of the cavity resonant frequencies. Also, f_a for the MM-CRDS case was more than five times smaller than $f_\mathrm{a} \simeq 100$ Hz which was achieved for the locked-cavity cases. The behavior of the SM-CRDS differs from the FS-CRDS only by a slow systematic drift which ultimately degrades sensitivity. In SM-CRDS there is typically no absolute frequency reference and consequently these spectra are expected to be subject to drifts that limit the length of time over which one can average ring-down data at a given probe laser frequency. In contrast for the FS-CRDS case, Fig. 3 illustrates that long-term averaging of the signal is not limited by drifts in the laser and/or cavity frequency. The NEA values are equal to $3.5 \times 10^{-9}\,\mathrm{cm}^{-1}\mathrm{Hz}^{-1/2}$, $1.2 \times 10^{-9}\,\mathrm{cm}^{-1}\mathrm{Hz}^{-1/2}$ and $7 \times 10^{-10}\,\mathrm{cm}^{-1}\mathrm{Hz}^{-1/2}$ for the MM-CRDS, SM-CRDS and FS-CRDS cases, respectively.

4.2 *Survey spectra and fitting of line shapes*

We completed a set of FS-CRDS spectra spanning the range $\tilde{\nu} = 7179.2053\,\mathrm{cm}^{-1}$ to $7183.5416\,\mathrm{cm}^{-1}$. Two spectra and their respective models are shown in Fig. 4. The spec-

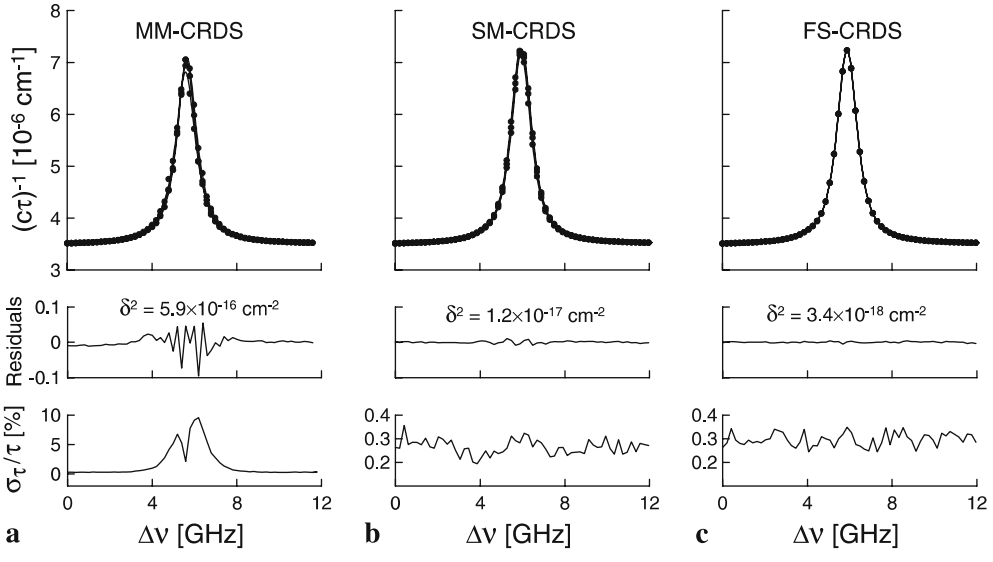

FIGURE 2 Left to right: (**a**) MM-CRDS, (**b**) SM-CRDS and (**c**) FS-CRDS cases. (*top panel*) Set of three ring-down spectra (*symbols*) and Galatry fits (*lines*) for each case. (*middle panel*) Fit residuals of one representative spectrum for each case. The term δ is the root-mean-square residual value. (*bottom panel*) Relative standard deviation of the measured time constants of one representative spectrum for each case. $\tilde{\nu} = 7181.156\,\mathrm{cm}^{-1}$ H_2O transition, $x = 4.3 \times 10^{-6}$, $p = 13.3$ kPa. $\Delta\nu = (\nu - \nu_0)$, $\nu_0 = 215\,279.68$ GHz for the FS-CRDS case

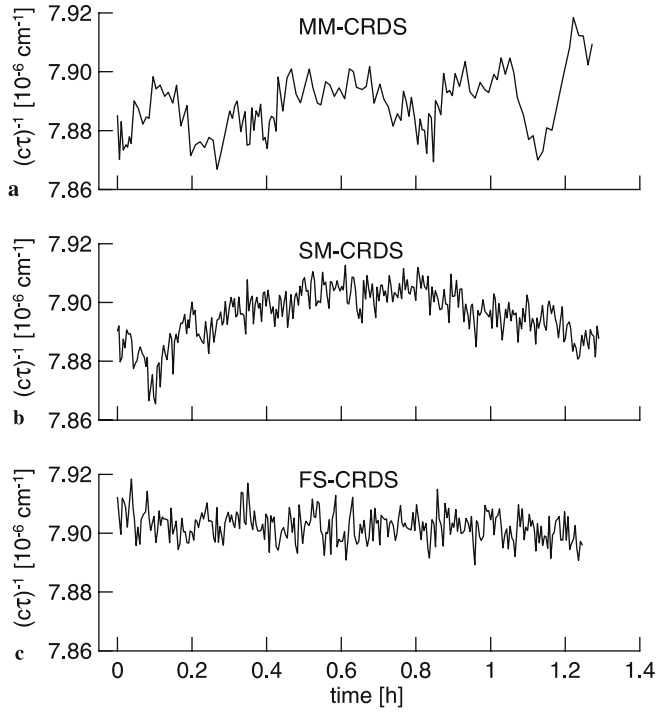

FIGURE 3 Temporal variation in the ring-down decay rate, $(c\tau)^{-1}$ near the line center for the (**a**) MM-CRDS, (**b**) SM-CRDS and (**c**) FS-CRDS cases. $\tilde{\nu} = 7181.156\,\mathrm{cm}^{-1}$ H_2O transition, $x = 4.3 \times 10^{-6}$, $p = 13.3\,\mathrm{kPa}$

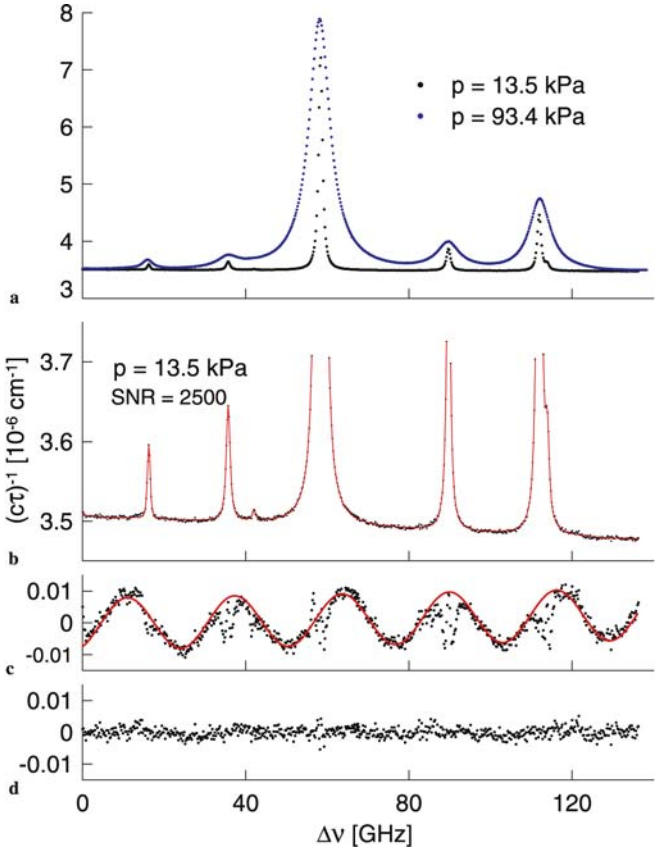

FIGURE 4 FS-CRDS survey spectra of H_2O absorption for $x = 4.3 \times 10^{-6}$. $\Delta\nu = (\nu - \nu_0)$, $\nu_0 = 215\,227.16$ GHz. (**a**) Measurements. (**b**) Expanded view with Galatry fits to measurements. (**c**) Residual étaloning structure (*symbols*) and sinusoidal fit (*line*). (**d**) Fit residuals after removing étaloning structure

tra correspond to $p = 93.4\,\mathrm{kPa}$ and $p = 13.5\,\mathrm{kPa}$, both with $x \simeq 4.3 \times 10^{-6}$ and measured $T = 296.9\,\mathrm{K}$. This region corresponds to the strongest water lines accessible with a commercially available DFB used for H_2O sensing. Near atmospheric pressure, these transitions are slightly blended and cannot easily be separated, whereas at substantially lower pressures, individual transitions can be identified. Each spectrum was modeled as a sum of nine Galatry profiles (all of which are previously assigned transitions) plus a baseline term. These transitions and their respective transition frequencies, quantum assignments and relative line intensities $s_i = S_i/S_\mathrm{m}$ (normalized by the line intensity of the strongest transition at $\tilde{\nu} = 7181.156\,\mathrm{cm}^{-1}$), are given in Table 1. The line intensity ratios measured at $T = 296.9\,\mathrm{K}$ are reported at the reference temperature $T = 296\,\mathrm{K}$, and were corrected for temperature-dependence of the respective line intensities using the HITRAN JavaHawks program and the HITRAN 2004 database [36]. This temperature correction changed the area ratio in all cases by less than 2%. In the analysis, all the Doppler widths were constrained to the expected values, as were the collisional narrowing parameters for the three weakest transitions. Other fitted parameters included the line intensities, frequency detunings and Lorentzian widths. Discussion of the fitted Lorentzian (broadening) widths and narrowing parameters given by the Galatry fits to the spectra is outside the scope of this paper. As discussed in [26], the Galatry gives a good representation of the $\mathcal{A}$, although speed-dependent effects on the line shape can not be neglected when interpreting the broadening and narrowing parameters obtained from

transition	$\tilde{\nu}_i$ (cm^{-1})	vibrational band	S_i (10^{-20} cm molecule^{-1})	Q'	Q''	$s_i = S_i/S_\mathrm{max}$	$\mathcal{A}_i/\mathcal{A}_\mathrm{max}$	$[\mathcal{A}_i/\mathcal{A}_\mathrm{max}]/s_i$
1	7179.752	$\nu_1+\nu_3$	0.0230	7,6,2	7,6,1	0.0153	0.0158	1.033
2	7180.400	$2\nu_1$	0.0561	3,2,1	4,1,4	0.0373	0.0380	1.019
3	7180.613	$\nu_1+\nu_3$	0.0030	9,5,5	9,5,4	0.00202	0.00284	1.406
4	7181.095	ν_1+2ν_2	0.0069	7,7,0	7,6,1	0.00456	0.00522	1.145
5	7181.156	$\nu_1+\nu_3$	1.5050	2,0,2	3,0,3	1	1	1
6	7182.156	$\nu_1+\nu_3$	0.0014	5,1,5	4,3,2	0.000912	0.000782	0.857
7	7182.209	$2\nu_1$	0.1541	1,0,1	1,1,0	0.102	0.106	1.039
8	7182.950	$\nu_1+\nu_3$	0.3752	2,1,2	3,1,3	0.249	0.253	1.016
9	7183.016	$\nu_1+\nu_3$	0.0412	2,0,2	2,2,1	0.0273	0.0265	0.971

TABLE 1 Summary of $H_2^{16}O$ transitions observed here. Assignments, positions and intensities taken from [36]. $Q\prime$ and $Q\prime\prime$ are rotational quanta of upper and lower states, respectively. The reported standard relative uncertainties in line intensities are from 5% to 10%. S_max and $\mathcal{A}_\mathrm{max}$ correspond to the reported line intensity and FS-CRDS-measured area for the transition $i = 5$ transition, respectively. Line intensities and ratios correspond to $T = 296\,\mathrm{K}$

a Galatry fit to the data. Interestingly, the periodic fit residuals for the low pressure spectrum indicate the occurrence of weak étaloning, and as shown previously [12], this baseline structure is consistent with an étalon corresponding to the optical pathlength difference between the curved and flat surfaces of the ring-down cavity mirrors. In the present case the mirrors were 3.9 mm thick with a refractive index = 1.5, thus yielding an étalon period $\simeq 26$ GHz. Refitting the low pressure spectrum, this time with a constrained baseline corresponding to the étaloning signature yields nearly unstructured residuals. Comparing the fitted line intensities (determined with and without the étaloning baseline term) indicates that incorporation of the étaloning effect can change the fitted values in $\mathcal{A}_i$ by as much as 1.5%: an important correction that if neglected would constitute a large measurement error. The $\mathcal{A}_i$ values were determined from the $p = 13.3$ kPa spectrum, and the ratio $[\mathcal{A}_i/\mathcal{A}_{\max}]/s_i$ is given in Table 1 for all the transitions. This ratio compares the measured and reported relative line intensities for these transitions. For the weakest transitions, the measured and reported intensity ratios differ by more than 40%. However, agreement between the FS-CRDS measurements and reported values of the relative line intensities is within 3.5% for the strongest transitions in this band.

To measure the H_2O concentration we restricted the spectral scan to the vicinity of the $\tilde{\nu} = 7181.156\,\mathrm{cm}^{-1}$ transition. Sample spectra obtained at $x \simeq 4.3 \times 10^{-6}$ and $p = 13.5$ kPa, 46.5 kPa and 93.4 kPa are shown in Fig. 5, along with the Galatry fit residuals for the $p = 46.5$ kPa case. The line shape fits included the two transitions labelled $i = 4$ and $i = 5$ given in Table 1, the latter being by far the dominant contributor to the spectrum. The results illustrate no systematic error in the lineshape within the signal-to-noise ratio (1000 : 1) of the measurements. The time dependence of x_{CRDS} and x_{CMH} are shown in Fig. 6. Both measurements respond similarly to a slight variation in the water vapor concentration associated with temperature drift in the PTMG system. After this perturbation, the relative standard deviation in x_{CRDS} is 0.12%, illustrating the high precision that can be achieved with the FS-CRDS technique when the water vapor concentration is sufficiently stable. The lower panel of Fig. 6 illustrates the degradation of precision associated with FS-CRDS vs. SM-CRDS. Here, the ring-down cavity frequency stabilization was terminated near the beginning of the data set, at which point the fluctuations in x_{CRDS} increase five-fold with respect to the FS-CRDS case.

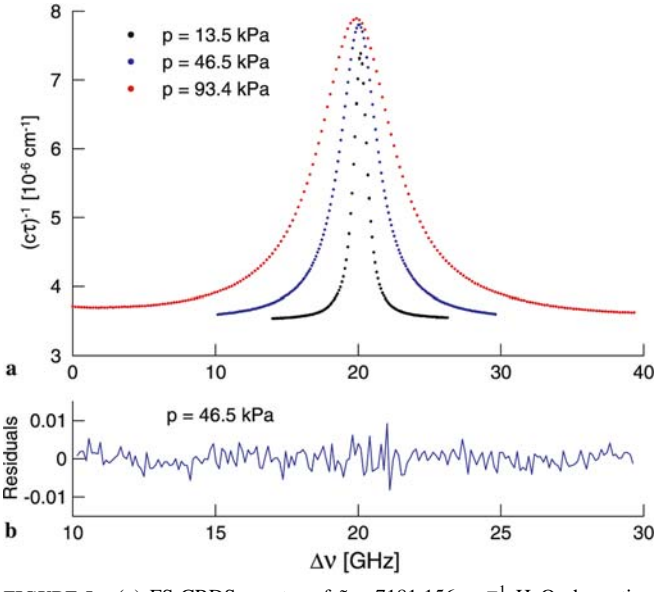

FIGURE 5 (**a**) FS-CRDS spectra of $\tilde{\nu} = 7181.156\,\mathrm{cm}^{-1}$ H_2O absorption for $x = 4.3 \times 10^{-6}$. $\Delta\nu = (\nu - \nu_0)$, $\nu_0 = 215\,265.41$ GHz. (**b**) residuals to $p = 46.5$ kPa case for Galatry line shape fit

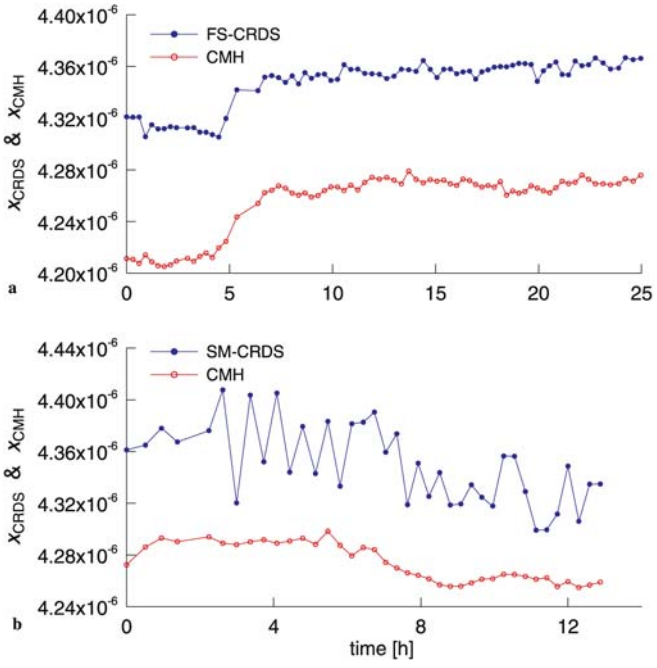

FIGURE 6 Time dependence of CRDS and CMH measurements of H_2O mole fraction produced by PTMG for $x = 4.3 \times 10^{-6}$. (**a**) FS-CRDS and CMH data. (**b**) SM-CRDS measurement (after the fifth data point) and CMH data

4.3 *Comparison of* FS-CRDS *with* CMH *measurements of water vapor*

To estimate the uncertainty of the FS-CRDS method we directly compared FS-CRDS and CMH measurements for the case $x \simeq 2.2 \times 10^{-6}$ and $p = 46.5$ kPa by probing the strong transition at $\tilde{\nu} = 7181.156\,\mathrm{cm}^{-1}$. For this comparison, we define the quantity $\Delta = (x_{\mathrm{CRDS}} - x_{\mathrm{CMH}})/x_{\mathrm{CMH}}$ to represent the relative difference between FS-CRDS and CMH measurements of x, where x_{CRDS} is based upon the temperature-corrected line intensity. This comparison can be confounded by differences between the water vapor background present in the ring-down cell and that of the chilled-mirror hygrometer. To account for background effects we define $x_{\mathrm{CRDS}} = x_{\mathrm{CRDS,obs}} - x_{\mathrm{CRDS,b}}$ and $x_{\mathrm{CMH}} = x_{\mathrm{CMH,obs}} - x_{\mathrm{CMH,b}}$ where $x_{\mathrm{CRDS,obs}}$ and $x_{\mathrm{CMH,obs}}$ are the respective observed values for the water vapor mole fraction and $x_{\mathrm{CRDS,b}}$ and $x_{\mathrm{CMH,b}}$ are the respective water vapor background values. Thus we define the apparent relative difference in measured water vapor concentration to be $\Delta_{\mathrm{obs}} = (x_{\mathrm{CRDS,obs}} - x_{\mathrm{CMH,obs}})/x_{\mathrm{CMH,obs}}$ which in the limit of zero water vapor background gives the quantity-of-interest Δ. In Fig. 7 we show that Δ_{obs} decays exponentially in time to an asymptotic value of 0.14% with a time constant $\simeq 24$ h. This slow time

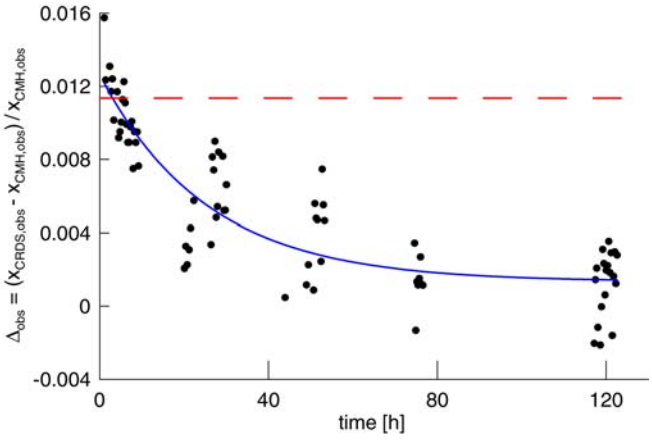

FIGURE 7 Relative difference (symbols) between CRDS and CMH measurements of H_2O mole fraction produced by PTMG defined by Δ_{obs}. $x = 2.2 \times 10^{-6}$, $p = 46.5$ kPa. The *solid line* is an exponential curve fit. The *dashed line* represents the value of Δ found by removing the asymptotic net water vapor background contribution given by $\Delta x_b = -2.1 \times 10^{-8}$

response is attributed to the equilibration of the water vapor concentration throughout the flow manifold and includes both the CMH and cavity ring-down sample volumes and all upstream plumbing. At equilibrium there is a net water vapor background given by $\Delta x_b = x_{CRDS,b} - x_{CMH,b}$ which is highly flow-manifold-geometry- and flow-rate dependent and which will bias the measurement of Δ_{obs} with respect to Δ. The respective background components, $x_{CRDS,b}$ and $x_{CMH,b}$ were determined by eliminating the PTMG water source and measuring the water vapor concentration in both the ring-down cell and CMH when exposed to dry N_2 ($x < 0.5 \times 10^{-9}$). To this end, the same total flow rate and gas pressure were considered as for the "wet" gas case in Fig. 7. After several days of equilibration, the background values of $x_{CRDS,b}$ and $x_{CMH,b}$ were measured to be $\simeq 4 \times 10^{-9}$ and 2.5×10^{-8}, respectively to give a net water vapor background $\Delta x_b = -2.1 \times 10^{-8}$. With the background at its asymptotic limit, the standard deviation in Δ_{obs} was less than 0.2%. The much larger water vapor background in the CMH compared to the ring-down cell was likely due to inadequate flushing of the sample lines. This difference exemplifies the technical challenge of hygrometry of ultra-dry sample streams, where care must be taken to minimize manifold-dependent sources/sinks of water vapor. The dashed line in Fig. 7 at 1.14% represents the value of Δ obtained after subtracting the asymptotic value of Δx_b. This background-corrected value of Δ shows a systematic difference between the CRDS and CMH measurements that is within the combined standard uncertainties of the reported line intensity and CMH measurements.

4.4 *Detection limit measurement*

We observed a relatively strong reduction in the laser beam intensity when probing the strong transition at $\tilde{\nu} = 7181.156\,\text{cm}^{-1}$ consistent with absorption by ambient water vapor in the nearly 1 m long external beam path. This effect required a lowering of the ring-down signal trigger threshold, which in turn caused a reduction in the signal-to-noise ratio and degradation in the measurement precision. To improve the measurements, the DFB output fiber was moved to within 20 cm of the ring-down cavity. In this configuration, we found that by removing the optical isolator which was normally located between the mode-matching lens and the ring-down cavity, the coupling efficiency of the probe laser beam into the ring-down cavity was greatly enhanced. This effect, which was likely caused by optical feedback from the ring-down cavity to the DFB laser, was repeatable and reduced $\sigma_\tau / \langle\tau\rangle$ to less than 0.1%, thus improving the measurement precision compared to the results given above. We note that controlled optical feedback from a folded (V-shaped) ring-down cavity to a DFB diode laser was recently demonstrated [33] using a servo loop that actuated a mirror located between the laser and cavity. In this context and with regard to our system, the observation that optical feedback improved the signal statistics deserves additional attention, and suggests that this effect can be controlled to optimize system performance.

Individual and averaged FS-CRDS spectra with Galatry fits corrected for the étaloning are shown in Fig. 8 for the configuration corresponding to having the isolator removed with concomitantly enhanced measurement statistics. The respective peak signal-to-noise ratios were $\simeq 5.5$ and 10 for the single spectrum and averaged spectrum. From these results we estimate a FS-CRDS detection limit $x < 0.7 \times 10^{-9}$ for a single scan of 10 min duration and 0.35×10^{-10} for an average of seven spectra over the course of 1 h. The single-spectrum results correspond to a NEA $= 1.2 \times 10^{-10}\,\text{cm}^{-1}\text{Hz}^{-1/2}$, evaluated at the absorption peak and assuming $f_{acq} = 100$ Hz. Finally, the detection limits reported here were limited by the relatively high transmission ring-down cavity mirrors given by $T_m \simeq 2.5 \times 10^{-4}$. Ring-down cavity mirrors with $T_m \simeq$

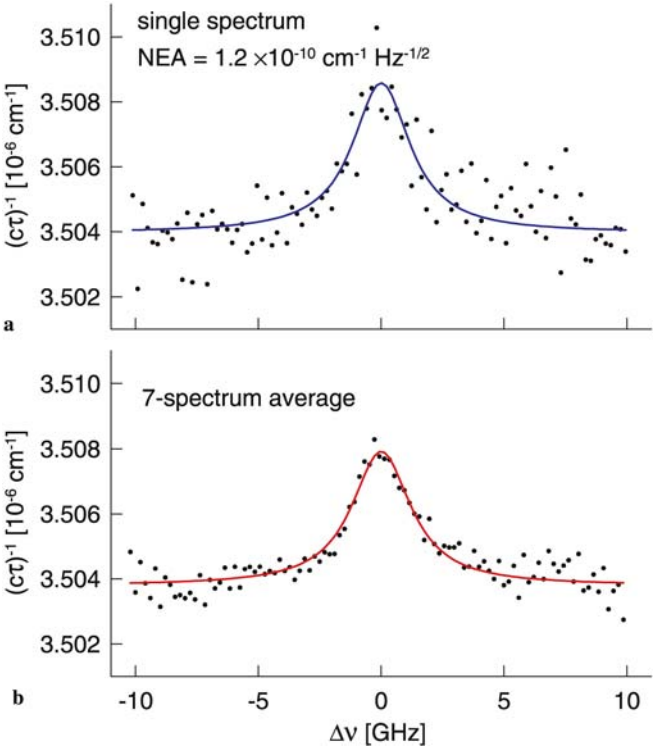

FIGURE 8 FS-CRDS spectra (*symbols*) of water vapor background in ring-down cavity. Galatry fits (*solid lines*). $x = 4 \times 10^{-9}$, $p = 46.5$ kPa. $\Delta\nu = (\nu - \nu_0)$, ν_0 = line center. $\tilde{\nu} = 7181.156\,\text{cm}^{-1}$ H_2O transition. (**a**) single spectrum. (**b**) average of seven spectra

1.5×10^{-5} are available and are expected to yield proportionally smaller values for the detection limit and NEA.

5 Conclusion

We have demonstrated the viability of FS-CRDS as an intrinsic spectroscopic standard of water vapor concentration by direct comparison of FS-CRDS to a standards-grade hygrometry apparatus. Systematic differences between the thermodynamic and spectroscopic measurements were dominated by water vapor background effects and uncertainty in line intensity, which are two factors with uncertainties that can be reduced. Future experiments, which will involve FS-CRDS measurements of water vapor samples generated by a primary standard generator [5] and linked to primary gravimetric methods, are expected to yield water vapor line intensities with improved accuracy. These data are necessary to make low uncertainty measurements of water vapor concentration from spectroscopic measurement of the line area, $\mathcal{A}$, without the need for further calibration or reference to other primary methods. Based on the present work, combined relative uncertainties in line intensity approaching the 0.25% level are achievable with the FS-CRDS technique. Finally, the portability of the FS-CRDS system makes it practical for a variety of laboratory and industrial applications in the measurement of trace quantities of water vapor.

ACKNOWLEDGEMENTS The authors would like to thank Howard P. Layer for his assistance in setting up the probe laser, Gregory E. Scace for his chilled-mirror hygrometry measurements, Randy Fink and Jim Yost for their help in setting up the water vapor sample system and finally Daniel Halmer for providing the software enabling the real-time fitting of the exponential decays. This work was supported by the NIST Office of Microelectronics Programs.

REFERENCES

1 P.L. Kebabian, C.E. Kolb, A. Freedman, J. Geophysic. Res. **107**, 4670 (2002)
2 J. Xie, B.A. Paldus, E.H. Wahl, J. Martin, T.G. Owano, C.H. Kruger, J.S. Harris, R.N. Zare, Chem. Phys. Lett. **284**, 387 (1998)
3 J. Wallace, Las. Focus World, March, 15 (2006)
4 H.H. Funke, B.L. Grissom, C.E. McGrew, M.W. Raynor, Rev. Sci. Instrum. **74**, 3909 (2003)
5 G.E. Scace, J.T. Hodges, Proc. Int. Symp. on Temperature and Thermal Measurements in Ind. and Sci. (TEMPMEKO 2001) (VDE Verlag, Berlin, 2002), pp. 597–602
6 A. O'Keefe, D.A.G. Deacon, Rev. Sci. Instrum. **59**, 2544 (1988)
7 G. Berden, R. Peeters, G. Meijer, Int. Rev. Phys. Chem. **19**, 565 (2000)
8 S.S. Brown, Chem. Rev. **103**, 5219 (2003)
9 A.J. Hallock, E.S.F. Berman, R.N. Zare, Anal. Chem. **74**, 1741 (2002)
10 R.L. Vander Wal, T. M Ticich, Appl. Opt. **38**, 1444 (1999)
11 A.W. Strawa, R. Castaneda, T. Owano, D.S. Baer, B.A. Paldus, J. Atmospher. Oceanic Technol. **20**, 454 (2003)
12 D. Romanini, K.K. Lehmann, J.Chem. Phys. **99**, 6287 (1993)
13 P. Zalicki, R.N. Zare, J. Chem. Phys. **102**, 2708 (1995)
14 J.T. Hodges, J.P. Looney, R.D. van Zee, J. Chem. Phys. **105 10**, 278 (1996)
15 K.K. Lehmann, D. Romanini, J. Chem. Phys. **105 10**, 263 (1996)
16 J.T. Hodges, J.P. Looney, R.D. van Zee, Appl. Opt. **35**, 4112 (1996)
17 J.P. Looney, J.T. Hodges, R.D. van Zee, Quantitative absorption measurements using cavity-ringdown spectroscopy with pulsed lasers, In: *Cavity-Ringdown Spectroscopy: An Ultratrace-Absorption Measurement Technique*, K.A. Busch, M.A. Busch (Eds.) (Oxford Univ. Press, 1998), Chapt. 7
18 R.D. van Zee, J.T. Hodges, J.P. Looney, Appl. Opt. **38**, 3951 (1999)
19 D. Romanini, A.A. Kachanov, N. Sadeghi, F. Stoeckel, Chem. Phys. Lett. **264**, 316 (1997)
20 D. Romanini, A.A. Kachanov, F. Stoeckel, Chem. Phys. Lett. **270**, 538 (1997)
21 A.R. Awtry, J.H. Miller, Appl. Phys. B **75**, 255 (2002)
22 M. Hippler, M. Quack, J. Chem. Phys. **116**, 6045 (2002)
23 J.B. Dudek, P.B. Tarsa, A. Velasquez, M. Wladyslawski, P. Rabinowitz, K.K. Lehmann, Anal. Chem. **75**, 4599 (2003)
24 P. Macko, D. Romanini, S.N. Mikhailenko, O.V. Naumenko, S. Kassi, A. Jenourvrier, Vl.G. Tyuterev, A. Campargue, J. Mol. Spectrosc. **227**, 90 (2004)
25 Tiger Optics, 250 Titus Ave., Warrington, PA, http://www.tigeroptics.com/
26 D. Lisak, J.T. Hodges, R. Ciuryło, Phys. Rev. A **73**, 012 507 (2006)
27 J.T. Hodges, H.P. Layer, W.W. Miller, G.E. Scace, Rev. Sci. Instrum. **75**, 849 (2004)
28 J.T. Hodges, R. Ciuryło, Rev. Sci. Instrum. **76**, 023 112 (2005)
29 D. Halmer, G. von Basum, P. Hering, M. Murtz, Rev. Sci. Instrum. **75**, 2187 (2004)
30 R.W. Hyland, A. Wexler, J. Res. NBS **77A**, 115 (1973)
31 A. Wexler, J. Res. NBS **81A**, 5 (1977)
32 T.G. Spence, C.C. Harb, B.A. Paldus, R.N. Zare, B. Willke, R.L. Byer, Rev. Sci. Instrum. **71**, 347 (2000)
33 J. Morville, S. Kassi, M. Chenevier, D. Romanini, Appl. Phys. B **80**, 1027 (2005)
34 R.Z. Martinez, M. Metsälä, O. Vaittinen, T. Lantta, L. Halonen, J. Opt. Soc. Am. B **23**, 727 (2006)
35 L. Galatry, Phys. Rev. **122**, 1218 (1961)
36 L.S. Rothman, D. Jacquemart, A. Barbe, D.C. Benner, M. Birk, L.R. Brown, M.R. Carleer, K. Chance, L.H. Coudert, V. Dana, V.M. Devi, J.-M. Flaud, R.R. Gamache, A. Goldman, J.-M. Hartmann, K.W. Jucks, A.G. Maki, J.-Y. Mandin, S.T. Massie, J. Orphal, A. Perrin, C.P. Rinsland, M.A.H. Smith, J. Tennyson, R.N. Tolchenov, R.A. Toth, J.V. Auwera, P. Varanasi, G. Wagner, J. Quantum Spectrosc. Radiat. Transf. **96**, 139 (2004)